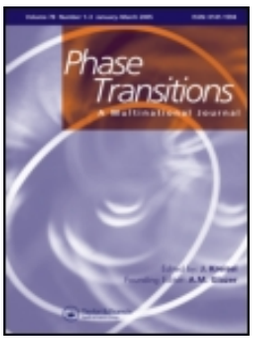

Taylor & Francis
Taylor & Francis Group

Phase Transitions
A Multinational Journal

ISSN: 0141-1594 (Print) 1029-0338 (Online) Journal homepage: https://www.tandfonline.com/loi/gpht20

Elastic percolation of swollen polyacrylamide (PAAm)–multiwall carbon nanotubes composite

Gülşen Akın Evingür & Önder Pekcan

To cite this article: Gülşen Akın Evingür & Önder Pekcan (2012) Elastic percolation of swollen polyacrylamide (PAAm)–multiwall carbon nanotubes composite, Phase Transitions, 85:6, 553-564, DOI: 10.1080/01411594.2011.634333

To link to this article: https://doi.org/10.1080/01411594.2011.634333

Phase Transitions
Vol. 85, No. 6, June 2012, 553–564

Taylor & Francis
Taylor & Francis Group

Elastic percolation of swollen polyacrylamide (PAAm)–multiwall carbon nanotubes composite

Gülşen Akın Evingür[a] and Önder Pekcan[b]*

[a]*Faculty of Science and Letters, Piri Reis University, 34940 Tuzla-İstanbul, Turkey;* [b]*Faculty of Science and Letters, Kadir Has University, 34083 Cibali-İstanbul, Turkey*

(*Received 12 August 2011; final version received 18 October 2011*)

Polyacrylamide (PAAm)–multiwalled carbon nanotube (MWNT) composites were prepared *via* free radical cross-linking copolymerization with different amounts of MWNTs varying in the range between 0.1 and 50 wt%. The mechanical properties of swollen PAAm–MWNT composites were characterized by the tensile testing technique. A small content of embedded nanotubes dramatically changes the compressive elastic modulus of the composites. Compressive elastic modulus dramatically increases up to 1 wt% MWNT on increasing nanotube content, and then decreases, presenting a critical MWNT value, indicating that there is a sudden change in the material elasticity. The critical exponent, y of elasticity, below the critical MWNT content, 1 wt%, is found to be 0.58, which is consistent with the suggestions of percolation in the *superelastic percolation network* for PAAm–MWNT composite.

Keywords: acrylamide; multiwalled-carbon nanotubes; hydrogel; mechanical properties

1. Introduction

Polymer composites can be used in many different forms in various areas ranging from structural units in the construction industry to the composites of the aerospace applications. The extraordinary properties of carbon nanotubes (CNTs) make them very promising and favorable as fillers for the fabrication of a new class of polymeric heterostructures. Polymer matrices have been widely exploited as a medium for CNTs, which have been described as effective conducting fillers for polymers. Nanotubes can be described as long and slender fullerenes, in which the walls of the tubes are hexagonal carbon (graphite structure). These tubes can either be single-walled carbon nanotube (SWNT) or multi-walled carbon nanotube (MWNT). Therefore, many researchers are focusing on the development of CNT-based polymer materials that utilize the CNT characteristics and properties, such as the high strength and stiffness of the CNTs, for developing superior polymer composites for structural applications which are lighter, stronger, and tougher than any other polymer-based materials. There are several important requirements for the effective improvement of CNT-based composites' properties, such as a large aspect ratio of a filler, good exfoliation, and dispersion of

*Corresponding author. Email: pekcan@khas.edu.tr

ISSN 0141–1594 print/ISSN 1029–0338 online

http://dx.doi.org/10.1080/01411594.2011.634333
http://www.tandfonline.com

nanotubes, and good nanotube–nanotube and nanotube–polymer interfacial bonding. Numerous studies have already shown that an effective performance of the CNTs in composites for a variety of applications strongly depends on the ability to homogenously disperse the CNTs throughout the matrix. Good interfacial bonding and interactions between nanotubes and polymers are also necessary conditions for improving mechanical properties of the composites. Due to the nanoscale size of the CNTs, the active CNT/matrix interface is significantly higher than that of other conventional fillers [1].

Bond percolation in elastic networks involving nearest neighbor forces was studied by numerical simulations. With purely central forces (CFs), the bulk and shear moduli go to zero, with exponent f, and at a threshold p_{cen} [2]. Elastic properties of random percolating systems in the critical region were studied by Kantor and Webman [3]. Critical exponent and transitions in swollen polymer networks and in linear macromolecules were studied by Erman and Flory [4], where the critical behavior was found for the single-chain and long-chain limits. Critical properties of viscoelasticity of gels and elastic percolation networks (EPNs) were modeled on the Zimm limit [5]. The scaling form for the correction dependence of viscosity in theta (θ) solvents and derivation of the concentration dependences of the modulus and longest relaxation time were explained by Colby and Rubinstein [6]. The viscosity and the modulus of near-critical polyester gels were reported and modeled by Rouse [7]. Scaling ideas were used to predict the modulus of the gels and equilibrium swelling of near-critical gels. The concentration dependence of the modulus when the gel was diluted in a good solvent was also calculated and used to predict the maximum swelling [8]. The strong stretching of network strands and its effect on modulus and equilibrium swelling were observed by Rubinstein et al. [9]. Elastic and osmotic behaviors and network imperfections of nonionic and weakly ionized acrylamide-based hydrogels were studied as a function of swelling degree Q and initial total monomer concentration. The shear modulus decreased as Q^{-m} at low Q and then steeply increased because network chains no longer obey Gaussian statistics [10]. Physical mechanism for the mechanical reinforcement in nanotube–polymer composite materials was presented and studied on the Frenkel–Kontorova model, which was potentially capable of predicting the ideal combination of polymers and nanotube diameters [11]. A review of modeling techniques for predicting the mechanical behavior of polymer nanocomposites was presented [12]. A detailed discussion of computational chemistry and computational mechanics modeling techniques is given. The mechanical properties of MWNT/poly(methyl methacrylate) (PMMA) nanocomposites were studied as a function of nanotube orientation, length, concentration, and type [13]. SWNT/PMMA nanocomposites were analyzed by optical microscopy, Raman imaging, and SEM, which were employed to determine the dispersion of nanotube at different length scales. Linear viscoelastic behavior and electrical conductivity of these nanocomposites were investigated [14]. A critical review on nanotube- and nanotube/nanoclay-related polymer composite materials was introduced in detail [15]. The relation between the structure and the viscoelastic behavior of a model polymer nanocomposite system based on a mixture of titanium dioxide nanoparticles and polypropylene was investigated. Above a critical volume fraction, the elasticity of the hybrids dramatically increased, and the frequency dependence of the elastic and viscous moduli reflected the superposition of the independent responses of the suspending polymer melt and of an elastic particle network [16].

The aim of this study is to understand the effect of MWNT content on the elastic behavior of swollen polyacrylamide (PAAm)–MWNT composite where the critical exponent of its elasticity was determined. In this study, composite gel systems are

produced by the inclusion of MWNTs, which are capable of converting the system from a liquid-like system to a solid-like one, when the amount of the MWNT addition exceeds a critical value known as the percolation threshold. The observed elasticity increased up to 1 wt% MWNT with the critical exponent around $y = 0.58$, which is indicative of the existence of *superelastic percolation network* (SEPN) in the composite gel. The elastic percolation threshold, 1 wt% agrees with the suggestions for the SEPN for the PAAm–MWNT composites.

2. Theory

2.1. *Elastic modulus in gels*

If a hydrogel is in the rubber-like region, then the elastic behavior of the gel is mainly dependent on the architecture of the polymer network. At low enough temperatures, these gels can lose their rubber elastic properties and exhibit viscoelastic behavior. General characteristics of rubber elastic behavior include high extensibility generated by low mechanical stress, complete recovery after removal of the deformation, and high extensibility and recovery that are driven by entropic rather than enthalpic changes.

To derive the relationship between the network characteristics and the mechanical stress–strain behavior, classical thermodynamics, statistical thermodynamics, and phenomenological approaches have been used to develop an equation of state for rubber elasticity. From classical thermodynamics, the equation of state for rubber elasticity may be expressed as [17]

$$f = \left(\frac{\partial U}{\partial L}\right)_{T,V} + T\left(\frac{\partial f}{\partial T}\right)_{L,V} \tag{1}$$

where f is the refractive force of the elastomer in response to a tensile force, U the internal energy, L the length, V the volume, and T is the temperature. For ideal rubber elastic behavior, the first term in Equation (1) is zero where changes in length cause internal energy-driven refractive forces. For elastomeric materials, an increase in length brings about a decrease in entropy because of changes in the end-to-end distances of the network chains. The refractive force and entropy are related through the following Maxwell equation

$$-\left(\frac{\partial S}{\partial L}\right)_{T,V} = \left(\frac{\partial f}{\partial T}\right)_{L,V} \tag{2}$$

Stress–strain analysis of the energetic and entropic contributions to the refractive force, Equation (1), indicates that entropy accounts for more than 90% of the stress. Thus, the entropic model for rubbery elasticity is a reasonable approximation.

From statistical thermodynamics, the refractive force of an ideal elastomer may be expressed as

$$f = -\left(\frac{\partial S}{\partial L}\right)_{T,V} = -kT\left(\frac{\partial \ln \Omega(r, T)}{\partial r}\right)_{L,V} \tag{3}$$

where k is the Boltzmann constant, r a certain end-to-end distance, and $\Omega(r, T)$ the probability that the polymer chain with an end-to-end distance r at temperature T will adopt a certain conformation. Equation (3) assumes that the internal energy contribution to the refractive force is constant or zero. Only entropy contributions to the refractive

force are considered. After evaluation of Equation (3), integration, and assuming no volume change upon deformation, the statistical thermodynamic equation of state for rubber elasticity is obtained below

$$\tau = \left(\frac{\partial A}{\partial \lambda}\right)_{T,V} = \frac{\rho RT}{\bar{M}_c}\frac{\overline{r_0^2}}{\overline{r_f^2}}\lambda \tag{4}$$

Here, τ is the shear stress per unit area, ρ the density of the polymer, $\overline{M_c}$ the number average molecular weight between cross-links, and λ the extension/compression ratio. Extension/compression ratio, λ, changes by different theory [18]. The quantity $\overline{r_0^2}/\overline{r_f^2}$ is the front factor and the ratio of the end-to-end distance in a real network to the end-to-end distance of isolated chains. In the absence of knowledge concerning these values, the front factor is often approximated as 1. From Equation (4), the elastic stress of a rubber under uniaxial extension/compression is directly proportional to the number of network chains per unit volume. This equation assumes that the network is ideal in that all chains are elastically active and contribute to the elastic stress. Network imperfections such as cycles, chain entanglements, and chain ends are not taken into account. To correct for chain ends

$$\tau = \frac{\rho RT}{\bar{M}_c}\frac{\overline{r_0^2}}{\overline{r_f^2}}\left(1 - \frac{2\overline{M_c}}{\overline{M_n}}\right)\lambda \tag{5}$$

where $\overline{M_n}$ is the number average molecular weight of the linear polymer chains before cross-linking. This correction becomes negligible when $\overline{M_n} \rangle\rangle \overline{M_c}$.

From constitutive relationship, the compressive elastic modulus $\boldsymbol{S}$ is then given by the following relation

$$S = \frac{\rho RT}{\bar{M}_c}\frac{\overline{r_0^2}}{\overline{r_f^2}}\left(1 - \frac{2\overline{M_c}}{\overline{M_n}}\right) \tag{6}$$

Here, the force per unit area is taken as

$$\tau = S\lambda \tag{7}$$

where $\lambda = \frac{\Delta l}{l_0}$, $\Delta l = l - l_0$; l, last distance and l_0, initial distance. Note the dependence of the compressive elastic modulus on $\overline{M_c}$. Also, the stress–strain behavior of rubbery elastic materials is nonlinear. The equations are less applicable and invalid at higher elongations ($\lambda > 3$) [19].

2.2. *Percolation on elastic networks*

Consider a percolation network whose bonds represent elastic springs that can be stretched and/or bent. The elastic energy of the system is given by [20]

$$E = \frac{\alpha_1}{2}\sum_{\langle ij \rangle}\left[\left(u_i - u_j\right)R_{ij}\right]^2 e_{ij} + \frac{\alpha^2}{2}\sum_{\langle jik \rangle}\left(\delta\theta_{jik}\right)^2 e_{ij}e_{ik} \tag{8}$$

where the first term on the right side represents the contribution of the stretching or CFs, whereas the second term represents the contribution of angle-changing or bond-bending (BB) force. Here α_1 and α_2 are the central and BB force constants, respectively, $u_i = (u_{ix}, u_{iy}, u_{iz})$ the (infinitesimal) displacement of site i, R_{ij} a unit vector from i to j, e_{ij} the

elastic constant of the (spring) between i and j, and $\langle jik \rangle$ indicates that the sum is over all triplets in which the bonds j–i and i–k form an angle whose vertex is at i. The change of angle $\delta\theta_{jik}$ is given by

$$\begin{aligned} \delta\theta_{jik} &= \left\{ \left(u_{ij} \times R_{ij} - u_{ik} \times R_{ik}\right) \cdot (R_{ik} \times R_{ik}) \Big/ \left| R_{ij} \times R_{ik} \right| \right. & R_{ij} \text{ not parallel to } R_{ik} \\ \delta\theta_{jik} &= \left\{ \left| \left(u_{ij} + u_{ik}\right) \times R_{ij} \right| \right. & R_{ij} \text{ parallel to } R_{ik} \end{aligned} \tag{9}$$

where $u_{ij} = u_i - u_j$. We can now define the elastic properties of percolation networks. Suppose that the elastic constants e_{ij} can be chosen from a distribution.

Each bond on disordered materials represents an elastic element, or a spring, with an elastic constant, e, and the rest have an elastic constant b, which can take on values from a probability density function $H(e)$. In most cases, $H(e)$ is written in terms of the binary distribution as

$$H(e) = p\delta(e - a) + (1 - p)\delta(e - b) \tag{10}$$

where e takes the values a and b with probabilities p and $1 - p$, respectively. If $b = 0$ and a is finite, the system is called EPN and S_e is defined as the effective compressive elastic modulus of the network. If $a = \infty$ and b is finite, a fraction p of the springs are totally rigid and the rest are soft, then the system is called a SEPN and S_s is defined as the effective compressive elastic modulus of a SEPN. As the percolation threshold p_c of an EPN is approached from above, S_e vanishes. Near the percolation threshold, p_c, the effective compressive elastic modulus of the network, S_e, obeys the following scaling law [20]

$$S_e(p) \approx (p - p_c)^x \tag{11}$$

where x is the critical exponent for EPN, whereas, S_s diverges as p_c is approached from below according to

$$S_s(p) \approx (p_c - p)^{-y} \tag{12}$$

where y is the critical exponent for SEPN and x and y are presented in Table 1, which includes critical exponents of elastic and SEPNs for three dimensions and in the mean field approximation [20].

Using this scaling description for S_e and S_s, upper and lower bounds for the exponent can be found

$$\Delta = \frac{x}{x + y} \tag{13}$$

If $x = 1.9$–2.1 can be used for the chemical gels and Equation (12) can be used for estimating y, it is obtained

$$0.61 \leq \Delta \leq 0.75 \tag{14}$$

where the lower and upper limits correspond to the Rouse and Zimm regimes, respectively.

Table 1. Critical exponents for elastic and SEPNs for three dimensions and in the mean field approximation [20].

	x	y
$d = 3$	2.1	0.65
$d \geq 6$	3	0

3. Experimental

3.1. *Preparation of composites*

We used MWNT which was analyzed by the Delta Nu Advantage 532 Raman Spectrometer with 100–3400 wave number spectral range (Cheap Tubes Inc., USA) with a length of range 20–30 nm and a diameter range of 10–30 nm. The purity of the MWNT was >95 wt%.

Initially, the stock solution is composed of MWNT, PVP, and water, in the proportions of 10 parts MWNTs: 1–2 parts PVP: 2000 parts distilled water at room temperature. The required dispersion time is approximately 5 or 6 min with an interruption of 10 s, every 30 s at full or high amplitude using ALEX ultrasonic equipment.

Composite gels were prepared using 2M AAm (Acrylamide, Merck) with various amounts, 0.1–50 wt%, of MWNT content at room temperature. AAm, the linear component; BIS (*N*,*N*′ methylenebisacrylamide, Merck), the cross-linker; APS (ammonium persulfate), the initiator; and TEMED (tetramethylethylenediamine, Merck), the accelerator were dissolved in distilled water. The solution was stirred (200 rpm) for 15 min to achieve a homogenous solution. All the samples were deoxygenated by bubbling nitrogen for 10 min just before the polymerization process.

3.2. *Mechanical characteristics measurements*

After gelation, the composites were cut into discs with $\approx$8.5 mm in diameter and $\approx$6 mm in thicknesses which are listed in Table 2. Before the compression measurements, the composites were maintained in water at 25°C to achieve swelling equilibrium. A final wash of all samples was made with deionized water for 1 week. Hounsfield H5K-S model tensile testing machine, settled a crosshead speed of 1.0 cm min^{-1} and a load capacity of 5 N, was used to perform uniaxial compression experiments on the samples of each type of composite gels. Figure 1 shows the behaviors of PAAm–MWNTs composite gels, before and after applying the uniaxial compression. Figure 1(a) and (b) shows the gel at

Table 2. Some experimental and calculated parameters of PAAm–MWNT composites.

PAAm (wt%)	MWNT (wt%)	*R* (mm)	*h* (mm)	*S* (MPa)
100	0	8.06	5.84	0.051
99.9	0.1	8.42	5.7	0.054
99.8	0.2	8.81	5.78	0.058
99.7	0.3	8.6	5.17	0.064
99.4	0.6	8.68	6.06	0.086
99	1	8.75	5.98	0.105
97	3	8.84	6.5	0.103
95	5	8.61	5.91	0.096
90	10	6.78	6.2	0.070
85	15	8.28	5.32	0.056
80	20	8.72	6.49	0.058
70	30	8.03	6.14	0.059
60	40	8.65	6.82	0.043
50	50	6.8	4.5	0.052

initial state, i.e., zero load and under 5 N, respectively. Any loss of water and changing in temperature during the measurements were not observed because the compression period was less than 1 min. There is no deswelling during the compressive deformation stage, which means that our experiment corresponds to the case where we can assume that the uniform compressive elastic modulus, S, is infinite. The compressive elastic modulus of each composite was determined from the slope of the linear portions of compression stress–strain curves, using Equation (7).

4. Results and discussion

Forces (F) or loads corresponding to compression (mm) were obtained from the original curves of uniaxial compression experiments. The force, F (N) *versus*, compression (mm) curves for 0.1 to 1 wt% MWNT content (low MWNT region) are shown in Figure 2(a), where it is seen that the repulsive force between atoms rapidly increases when compression

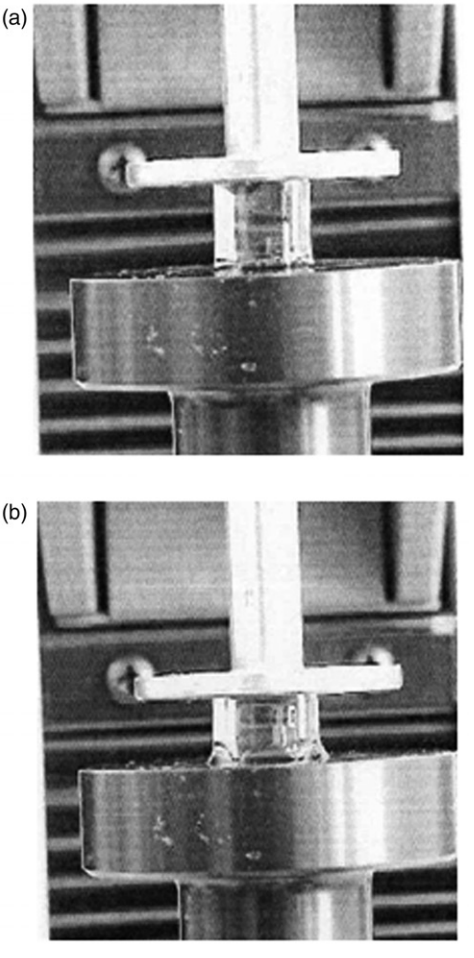

Figure 1. Loading processes of 0.1 wt% MWNT content composite gel at: (a) initial ($F = 0.0$ N) and (b) final ($F = 5.0$ N) states.

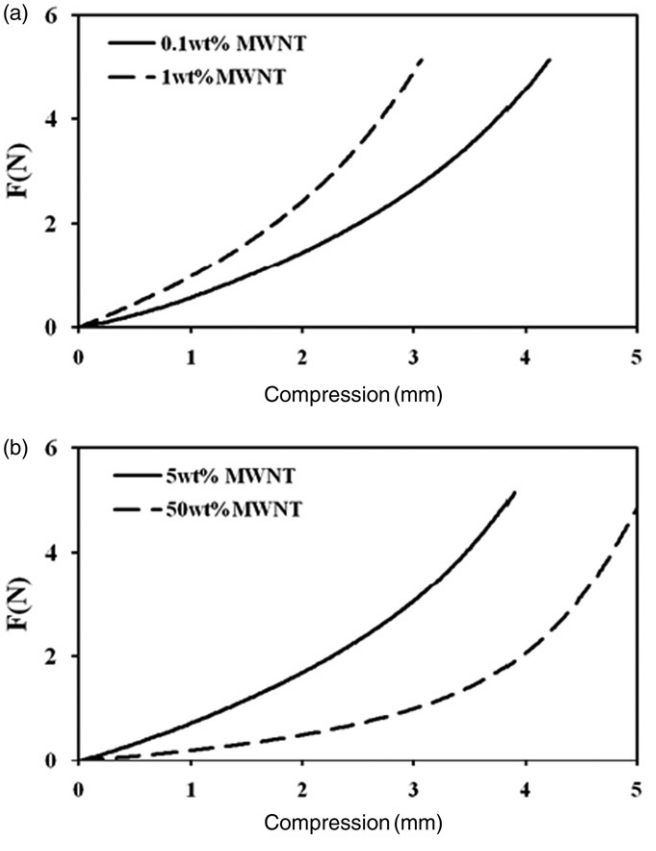

Figure 2. The force F (N) *vs*. compression (mm) curves for: (a) 0.1–1 wt% MWNT contents and (b) 5–50 wt% MWNT contents at 25°C, respectively.

is increased, i.e., the bond length is shortened with respect to the equilibrium position. If MWNT content is increased in low MWNT region, then repulsive force increased much slowly for the high MWNT content sample, as shown in Figure 2(a) [21]. On the other hand, Figure 2(b) shows the F (N) *versus* compression (mm) curves for 5–50 wt% MWNT content (high MWNT region), presenting the reverse behavior compared to low MWNT region.

Stress (Pa)–Strain plots of low and high MWNT content gels produced using the data obtained from the linear region, in the plots of F (N) *versus* compression curves for PAAm–MWNT composites at 25°C, are shown in Figure 3(a) and (b), respectively. The stress *versus* strain displays a good linear relationship at 25°C, which agrees with Equation (7). The compressive elastic moduli were obtained by a least square fit to the linear region and are listed in Table 2. For pure PAAm gels, the value of the compressive elastic modulus is found to be 0.051 MPa. The addition of MWNT into PAAm caused an increase in compressive elastic modulus of the composite as expected. In PAAm–1 wt% MWNT composite, the measured compressive elastic modulus is found to be 0.105 MPa, two times larger than pure PAAm sample. It is seen in Figure 3(a) that PAAm–0.1 wt% MWNT composite has smaller initial slope than 1 wt% MWNT content composite. In this case, it appears that the alignment effect of MWNT plays an important role for getting the

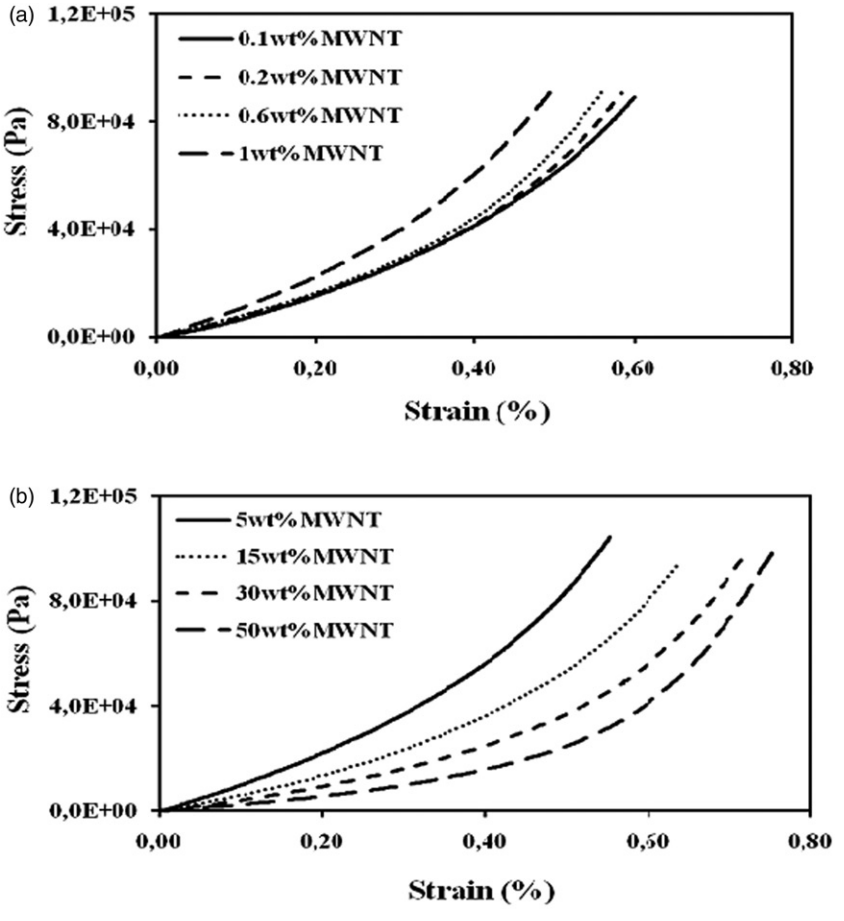

Figure 3. Stress and strain curves for: (a) lower and (b) higher MWNT contents.

different onset behavior [22]. The stress of the PAAm–MWNT (1–5 wt% MWNT composites) dramatically increases when the strain exceeds 0.6%, where the alignment is taking place in the composite. On the other hand, at high MWNT region, the random motion of MWNT impedes alignment, as predicted in Figure 3(b). Therefore, in a gel with low MWNT content, alignment of MWNTs with each other is much easier than that in high-content MWNT composite.

Figure 4 shows the plot of compressive elastic modulus, $\boldsymbol{S}$ *versus* MWNT content in the composite gel. Compressive elastic modulus dramatically increases up to 1 wt% MWNT with the increase in nanotube content, and decreases presenting a critical MWNT value, indicating that there is a sudden change in the material elasticity. The sudden change in $\boldsymbol{S}$ predicts that the composites have reached a SEPN [14]. At contents above 1 wt% MWNTs, the compressive elastic modulus is marginally decreased with increasing MWNT content. On the other hand, at low MWNT content ($\leq$1 wt%), the compressive elastic modulus increases up to 0.105 MPa, only exceeding it when the MWNT content is above 1 wt% and then decreases further as the MWNT content is raised. At the percolation threshold, 1 wt% of the nanotubes form an interconnecting structure, called percolation

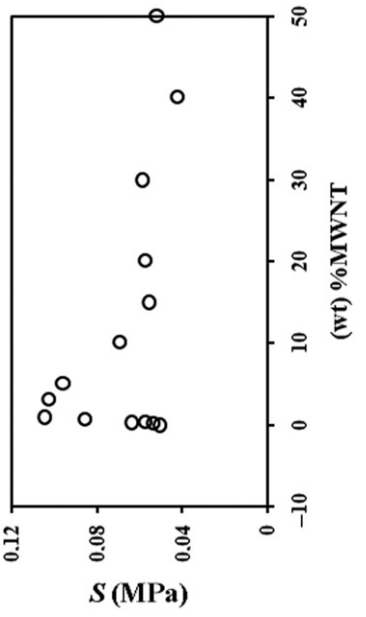

Figure 4. Dependence of compressive elastic modulus on content of wt% MWNT in the composite.

cluster exhibiting a high degree of nanotube interactions and/or entanglement [23]. The increasing MWNT content produces infinite network, reducing the swelling and decreasing compressive elastic modulus, as expected for the composites at high MWNT content. The decrease in elastic modulus, S, can be explained by the formation of a CNT network, which significantly improves the stiffness of composite gel., i.e, due to the high stiffness, the mechanical properties should be substantially influenced [24]. On the other hand, when the MWNT content is below 1 wt%, the compressive elastic modulus presents lower values and increases as MWNT is added. It is believed that the mechanical properties of MWNT–polymer composites are highly dependent on nanotube dispersion, which directly influences the molecular tube–tube and tube–polymer interactions in the composites. Such molecular interactions will play a critical role in load transfer and interfacial bonding that determines mechanical properties of the composites. The variations in the nanotube dispersion in the resultant composite could be the major reason for this phenomenon [22].

In Figure 4, it is understood that 1 wt% is the critical percolation threshold, p_c at which gel system owns a percolation cluster formed from MWNTs. Here, the composite gel passes the highest elasticity presenting the highest $\boldsymbol{S}$ value. Equation (12) now can be used to fit the $\boldsymbol{S}$ *versus* wt% MWNT curve below the critical point (below 1 wt%). The value of the fitting exponent y in Equation (12) was estimated from the slope of the linear relation between log $\boldsymbol{S}$ and log $Ip - p_cI$, as shown in Figure 5. Elastic percolation occurs below 1 wt% MWNTs (Figure 4) with a critical exponent around $y \approx 0.58$, which is close to the theoretical prediction of this value in the 3D percolated system known as a SEPN. The critical exponent, y, agrees with the literature values (Table 1) [20]. Here, x is the critical exponent which is taken from literature by the upper limit $x \approx 2.1$. Moreover, Δ was found to be 0.74, very close to the upper limit of Δ, as given in Equation (14).

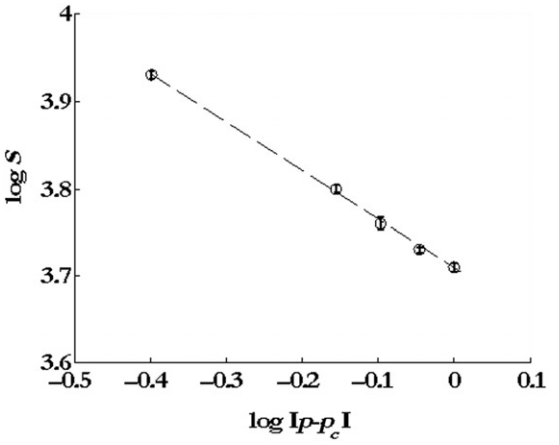

Figure 5. Logarithmic plot of the compressive elastic modulus *vs.* MWNT contents curves for $p < p_c$. The exponent, y was determined from the slope of the straight line.

5. Conclusions

The mechanical measurements were performed in PAAm–MWNT composites using a tensile testing machine. The elastic percolation threshold occurs at 1 wt% MWNT in the composite system. The critical exponent y obtained from fitting the MWNT dependence of the compressive elastic modulus below the elastic percolation threshold, 1 wt%, is consistent with the SEPN model for PAAm–MWNT composite. It is observed that below and above the percolation threshold PAAm–MWNT composite produced lower $\boldsymbol{S}$ values. Below the highest $\boldsymbol{S}$, the composite system acts as SEPN. However, above this critical value, the composite presents high stiffness due to the infinite MWNT network formed with high MWNT contents.

Acknowledgments

Prof. Dr Önder Pekcan thanks TÜBA for providing financial support. The authors thank Dr Argun Talat Gökçeören for mechanical measurements.

References

[1] M. Olek, *Carbon Nanotube Composites Mechanical, Electrical and Optical Properties*, Mathematics and Nature Department, Bonn University, Bonn, Germany, 2006.
[2] S. Feng and P.N. Sen, *Percolation on elastic networks: New exponent and threshold*, Phys. Rev. Lett. 52(3) (1984), pp. 216–219.
[3] Y. Kantor and I. Webman, *Elastic properties of random percolating systems*, Phys. Rev. Lett. 52(21) (1984), pp. 1891–1894.
[4] B. Erman and P.J. Flory, *Critical phenomena and transitions in swollen polymer networks and in linear macromolecules*, Macromolecules 19 (1986), pp. 2342–2353.
[5] S. Arbabi and M. Sahimi, *Critical properties of viscoelasticity of gels and elastic percolation networks*, Phys. Rev. Lett. 65(6) (1990), pp. 725–728.
[6] R.H. Colby and M. Rubinstein, *Two parameter scaling for polymers in theta solvents*, Macromolecules 23 (1990), pp. 2753–2757.

[7] R.H. Colby, J.R. Gillmor, and M. Rubinstein, *Dynamics of near critical polymer gels*, Phys. Rev. E 48(5) (1993), pp. 3712–3716.
[8] M. Rubinstein and R.H. Colby, *Elastic modulus and equilibrium swelling of near critical gels*, Macromolecules 27 (1994), pp. 3184–3190.
[9] M. Rubinstein, R.H. Colby, and A.V. Dobrynin, *Elastic modulus and equilibrium swelling of polyelectrolyte gels*, Macromolecules 29 (1996), pp. 398–406.
[10] S.A. Dubrovskii and G. Rakova, *Elastic and osmotic behavior and network imperfections of nonionic and weakly ionized acrylamide based hydrogels*, Macromolecules 30 (1997), pp. 7478–7486.
[11] A. Wall, J.N. Coleman, and M.S. Ferreira, *Physical mechanism for the mechanical reinforcement in nanotube-polymer composite materials*, Phys. Rev. B 71 (2005), pp. 125421(1–5).
[12] P.K. Valavala and G.M. Odegard, *Modeling techniques for determination of mechanical properties of polymer nanocomposites*, Rev. Adv. Mater. Sci. 9 (2005), pp. 34–44.
[13] R.E. Gorga and R.E. Cohen, *Toughness enhancements in poly(methyl methacrylate) by addition of oriented multiwalled carbon nanotubes*, J. Polym. Sci., Part B: Polym. Phys. 42 (2004), pp. 2690–2702.
[14] F. Du, R.C. Scogna, W. Zhou, S. Brand, J.E. Fischer, and K. Winey, *Nanotube networks in polymer nanocomposites: Rheology and electrical conductivity*, Macromolecules 37 (2004), pp. 9048–9055.
[15] K. Lau, C. Gu, and D. Hui, *A critical review on nanotube and/nanoclay related polymer composite materials*, Composites Part B 37 (2006), pp. 425–436.
[16] G. Romeo, G. Fillippone, A.F. Nieves, P. Russo, and D. Acierno, *Elasticity and dynamics of particle gels in non-newtonian melts*, Rheol. Acta 47 (2008), pp. 989–997.
[17] L.R.G. Treloar, *The Physics of Rubber Elasticity*, 3rd ed., Clarendon Press, Oxford, 1975.
[18] L.E. Nielsen and R.F. Landel, *Mechanical Properties of Polymers and Composites*, Marcel Dekker, New York, NY, 1994.
[19] K.S. Anseth, C.N. Bowman, and L.B. Peppas, *Mechanical properties of hydrogels and their experimental determination*, Biomaterials 17 (1996), pp. 1647–1657.
[20] M. Sahimi, *Application of Percolation Theory*, Taylor and Francis, London, 1994.
[21] T. Natsuki and M. Endo, *Stress simulation of carbon nanotubes in tension and compression*, Carbon 42 (2004), pp. 2147–2151.
[22] K. Awasthi, S. Awasthi, A. Srivastava, R. Kamalakaran, S. Talapatra, P.M. Ajayan, and O.N. Srivastava, *Synthesis and characterization of carbon nanotube-polyethylene oxide composites*, Nanotechnology 17 (2006), pp. 5417–5422.
[23] P. Pötschke, T.D. Fornes, and D.R. Paul, *Rheological behavior of multiwalled carbonnanotube/polycarbonate composites*, Polymer 43 (2002), pp. 3247–3255.
[24] O. Meincke, D. Kaempfer, H. Weickmann, C. Friedrich, M. Vathauer, and H. Warth, *Mechanical properties and electrical conductivity of carbon-nanotube filled polyamide-6 and is blends with acrylonitrile/butadiene/styrene*, Polymer 45 (2004), pp. 739–748.